

# TEANet: A Transpose-Enhanced Autoencoder Network for Wearable Stress Monitoring

Md Santo Ali, *Student Member, IEEE*, Sapnil Sarker Bipro, *Graduate Student Member, IEEE*,  
 Mohammad Abdul Motin, *Senior Member, IEEE*, Sumaiya Kabir, *Member IEEE*,  
 Manish Sharma, *Senior Member, IEEE*, M. E. H. Chowdhury, *Senior Member, IEEE*

**Abstract**— Mental stress poses a significant public health concern due to its detrimental effects on physical and mental well-being, necessitating the development of continuous stress monitoring tools for wearable devices. Blood volume pulse (BVP) sensors, readily available in many smartwatches, offer a convenient and cost-effective solution for stress monitoring. This study proposes a deep learning approach, a Transpose-Enhanced Autoencoder Network (TEANet), for stress detection using BVP signals. The proposed TEANet model was trained and validated utilizing a self-collected RUET SPML dataset, comprising 19 healthy subjects, and the publicly available wearable stress and affect detection (WESAD) dataset, comprising 15 healthy subjects. It achieves the highest accuracy of 92.51% and 96.94%, F1 scores of 95.03% and 95.95%, and kappa of 0.7915 and 0.9350 for RUET SPML, and WESAD datasets respectively. The proposed TEANet effectively detects mental stress through BVP signals with high accuracy, making it a promising tool for continuous stress monitoring. Furthermore, the proposed model effectively addresses class imbalances and demonstrates high accuracy, underscoring its potential for reliable real-time stress monitoring using wearable devices.

Source Code: <https://github.com/shantoruetee19/TEANet-ruet-spml>

**Index Terms**— Convolutional neural network, explainable machine learning, blood volume pulse signal, stress monitoring, wearable devices.

## I. INTRODUCTION

STRESS is the organism's response to any change that induces physical or psychological strain and pressure, with the body's reactions, referred to as stress responses, being nonspecific and manifesting physiologically, behaviorally, and emotionally [1], [2]. Mental stress can manifest as physical and mental health issues, including cardiovascular disease, depression, and anxiety, making its recognition crucial due to

the potential negative impact on overall health prompting individuals to monitor their stress levels in daily life. Stress detection involves analyzing facial expressions, text-based assessments, and physiological signals [3], [4], [5], but the former methods are limited by variability, subjectivity, and external factors, making physiological signals more reliable for objective and real-time monitoring. A variety of physiological signals, including electrocardiogram (ECG) [6], [7], electromyogram (EMG) [8], skin temperature (TEMP) [8], BVP [7], [9], [10], electrodermal activity (EDA) [9], acceleration (ACC) [8], respiration (RESP) [8], heart rate variability [10] and electroencephalogram (EEG) [11], have been extensively studied for stress monitoring, both individually and in combination, using diverse processing techniques and statistical or machine learning methods.

While EEG effectively reflects brain activity changes during mental stress, its practical application is hindered by the inconvenience and cost of EEG headsets and electrodes placed on the body of subjects [12]. Similarly, EMG, requiring muscle attachment, is impractical for widespread use [13]. ECG provides a non-invasive way to monitor electrical activity of heart and detect stress-related changes in heart rate variability, but it is often expensive and cumbersome due to the need for multiple electrodes and specialized equipment [6], [14-16]. Commercial wearable devices primarily use BVP sensors for physiological monitoring due to their affordability [17]. Moreover, BVP has emerged as a viable alternative to ECG for physiological assessments, offering a non-invasive approach while effectively measuring heart rate and variability [18-23].

The use of machine learning (ML) and deep learning (DL) techniques for analyzing BVP signals has become a prominent approach in stress monitoring. Several studies [8], [10], [24-30] have explored ML based approaches for stress monitoring using BVP signals, either independently or in combination with other physiological signals. Traditional approaches typically rely on hand-crafted features, including temporal, frequency-domain, non-linear, and statistical features. Benckekroun *et al.* [24] compared the performance of stress classification using ECG and BVP signals by RF classifier. Additionally, studies [8], [10], [27-29] investigated multimodal approaches, incorporating BVP alongside other physiological signals for stress classification using traditional ML techniques. These studies leveraged signals such as EDA, RESP, HRV, ECG, ACC, and EMG alongside BVP signals. Zhu *et al.* [29] compared EDA, ECG, and BVP signals individually and

Md Santo Ali, Sapnil Sarker Bipro, Mohammad Abdul Motin, and Sumaiya Kabir are with Department of Electrical & Electronic Engineering, Rajshahi University of Engineering & Technology, Bangladesh (Correspondence e-mail: [m.a.motin@ieee.org](mailto:m.a.motin@ieee.org)).

Sumaiya Kabir is also with the School of Engineering, RMIT University, Melbourne, Australia ([sumaiya.kabir.1993@ieee.org](mailto:sumaiya.kabir.1993@ieee.org)).

Manish Sharma is with the Electrical and Computer Science Engineering, Institute of Infrastructure, Technology, Research and Management (IITRAM), Ahmedabad, Gujarat, India ([manishsharma@iitram.ac.in](mailto:manishsharma@iitram.ac.in)).

M. E. H. Chowdhury is with Electrical Engineering Department, Qatar University, Doha-2713, Qatar ([mchowdhury@qu.edu.qa](mailto:mchowdhury@qu.edu.qa)).

combined, reporting a peak accuracy of 86.4% using a stacking ensemble with EDA. The studies in [8], [10], and [27] focused exclusively on multimodal signals, alongside BVP. Bobade *et al.* [8] utilized the maximum number of signals in their study, extracting features from ACC, ECG, BVP, EDA, EMG, RESP, and TEMP. Mozos *et al.* [10] extracted features from BVP, and EDA, while Can *et al.* [27] used BVP, EDA, and ACC. Among these studies, the highest reported accuracy of 95.21% in the binary classification of stress classification was achieved by Bobade *et al.* [8], relying on features from seven modalities. Stress classification in studies [25, 26], and [30] was conducted exclusively using BVP signals. Beh *et al.* [30] introduced an outlier removal technique for the BVP signal, whereas Heo *et al.* [26] proposed a complex denoising and peak detection method. While the method proposed by Heo *et al.* significantly enhances classification accuracy, it involves a highly complex preprocessing technique. However, traditional ML methods often rely on human expertise, known as feature engineering, which can be time-consuming, error-prone, and require domain knowledge. Additionally, these methods may struggle to capture complex, non-linear relationships within the data, especially as the dataset grows.

A plethora of DL-based models have been explored for mental stress assessment [9], [7], [31-38]. Among these, [9], [7], [32, 34-36] focused on hybrid model-based stress classification using hand-crafted features and frequency domain 2D images, employing either unimodal BVP signals or multimodal signals that include BVP. Henry *et al.* [7] assessed the generalizability of BVP and ECG signals across various datasets, while Gasparini *et al.* [34] employed 2D scalograms and hand-crafted features, and Elzeiny *et al.* [32] utilized spatial and frequency domain images. Conversely, several studies, [31, 33, 37, 38] directly fed BVP or multimodal BVP signals into DL models. Hasanpoor *et al.* [33] achieved a peak accuracy of 82% using a CNN-MLP architecture on unimodal BVP data. Li *et al.* [31], and Alshamrani [38] explored multimodal BVP with CNN and fully convolutional network (FCN)-based approaches, respectively. Furthermore, Chen *et al.* [37] evaluated the performance of unimodal, bimodal, and trimodal signal configurations for stress classification using three distinct deep learning-based models. The study utilized signals such as BVP, ECG, and EEG, demonstrating the comparative effectiveness of each modality in the classification task.

Deep learning-based models, generally, outperform traditional machine learning-based models by effectively processing raw data and automatically extracting relevant features [39], [40]. Many studies utilize either hand-crafted features or images obtained by means of fast Fourier transform (FFT), short term fast Fourier transform or some other joint time-frequency methods. The manual feature extraction process, however, may discard important information, leading to suboptimal performance. Additionally, converting time-series data into images can significantly increase computational complexity. When combined with deep learning, such approaches may limit the model's potential in real time applications. Given the computational constraints and real-time requirements of wearable devices, we hypothesize that

processing unimodal BVP data with deep learning models installed in wearable devices can be the optimal approach for stress assessment.

This study introduces a transpose-enhanced autoencoder network for stress monitoring from BVP signals. The primary objective of this research is to develop a high-performance unimodal DL-based solution for real-world stress monitoring. The key contributions of this work are as follows:

- A novel transpose-enhanced autoencoder network (TEANet) model for stress monitoring using wearable device-derived BVP signals, capable of delivering balanced performance on highly imbalanced datasets while outperforming existing state-of-the-art approaches.
- A sliding window segmentation-based augmentation strategy to address the class imbalance between normal and stressed classes.
- Creation of a private dataset, followed by comprehensive model verification using both public dataset and private dataset created by us for this study.
- Furthermore, to ensure model generalizability and robustness, we employed subject-independent leave-one subject-out (LOSO) validation.

This paper is organized as follows: Section II describes the materials and methods, Section III presents the results and discussion, and Section IV concludes the proposed study.

## II. MATERIALS AND METHODS

This section provides a complete overview of the dataset and data recording procedure, signal preprocessing, and proposed deep learning model deployment for stress classification, followed by detailed subsections.

### A. Dataset Description

In this study, we validated our proposed model using two datasets. Firstly, we conducted an experiment to collect physiological data from 19 participants, and the dataset was named after our research group, the Signal Processing and Machine Learning Research (SPML) Group at Rajshahi University of Engineering & Technology (RUET), referred to as the RUET SPML stress dataset. Additionally, we utilized the publicly available wearable stress and affect detection (WESAD) dataset [41]. We validated our proposed model on both the publicly available and the private dataset, improving its robustness and generalizability. The details of these datasets are provided below.

1) **RUET SPML Dataset:** We selected a total of 22 healthy participants, predominantly consisting of undergraduate students, graduates, and faculties affiliated with the Rajshahi University of Engineering and Technology (RUET). Prior to signal collection, we obtained ethical approval from the university authorities, and each participant provided a written consent. Due to sensor malfunctions, data from three sets of signals were excluded from our analysis. The remaining 19 subjects ranged from 21 to 36 years. The device used in this study was the Empatica E4 wristband (Fig. 1), a wrist-worn device that stores the collected data in the cloud. The signals collected included BVP, EDA, TEMP, and ACC with the sampling frequency of 64, 4, 4, and 32 Hz, respectively. In our

experiment, we focused only on the BVP signal. A demographic summary focusing on the BVP signal from the RUET SPML dataset is presented in Table I.

TABLE I  
SUMMARY OF THE DEMOGRAPHIC INFORMATION FOR BVP SIGNAL IN RUET SPML DATASET

Item	Information
Subjects	19
Gender (M/F)	15 Male & 4 Female
Age (mean $\pm$ SD)	24 $\pm$ 2.8
Trials per subject	4
Total trials	115
Total duration	230 minutes (approx..)
Sampling frequency	64Hz (BVP)

\*Standard Deviation (SD)

Before data collection, participants were instructed to abstain from consuming caffeine and tobacco for at least one hour and avoid prospective activities. Each participant provided written consent before data collection. The study protocol, data collection procedure, and application of the study were briefed to the participants. The study protocols and data collection procedure are detailed below and illustrated in Fig. 1.

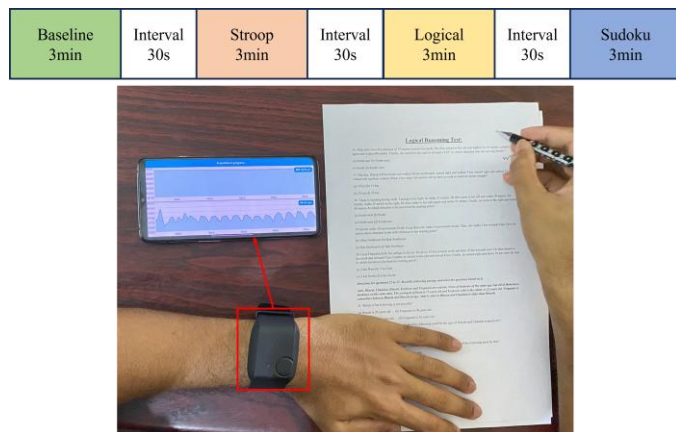


Fig. 1. The study protocol consists of a baseline condition lasting 3 minutes, followed by three stress-inducing tasks: Stroop, logical reasoning, and Sudoku tests, each lasting 3 minutes. A 30-second interval is incorporated between each task to allow participants to reset before the next stimulus. The signal collection procedure using the Empatica E4 wristband is illustrated, highlighting the timing and sequence of the conditions.

Each participant was exposed to three distinct stimuli. A 30-second interval was incorporated between stimuli, serving as a preparatory phase to ensure synchronization between the device and the stimuli. Each stimulus was administered for 3 minutes.

- **Baseline Condition:** Before applying any stimuli, 3 minutes of data were recorded as the baseline data described in [41-44]. During this time, participants were instructed to remain calm and stress-free.
- **Stroop Test:** After the baseline session, participants undertook the Stroop test, following protocols described in [45] and adapted as outlined in [46]. This test assesses interference in cognitive processing through two main factors: the color of the stimulus (ink color of the word) and the semantic meaning of the word [35]. Participants were presented with a sheet containing color names printed in incongruent ink colors and were instructed to identify the ink color while ignoring the word itself.

- **Logical Task:** The next cognitive load was applied through a logical task [43]. The logical tasks included a variety of low-complexity intelligence questions and arithmetic problems, designed to be completed within a limited time frame. This test aimed to further induce mental stress by challenging participants' reasoning abilities and quick thinking under time constraints.
- **Sudoku Task:** The final assessment involved a Sudoku task, incorporating stress induction methods inspired by Chen *et al.* [37], Gergelyfi *et al.* [47] and Weiqi *et al.* [48]. The Sudoku-solving task requires cognitive engagement, which serves as a source of mental stress. The objective of the Sudoku puzzle is to fill the cells of a  $9 \times 9$  grid with digits from 1 to 9, ensuring that each digit occurs only once in each row and column.

2) **WESAD Dataset:** The WESAD dataset comprises physiological, and motion data collected from 17 participants wearing wearable sensors. Due to sensor malfunctions, data from two participants were excluded. Among the 15 participants, 12 were males and 3 were females, with a mean age of  $27.5 \pm 2.4$  years. This dataset encompasses eight modalities captured by two devices: RespiBAN (chest-worn) and Empatica E4 (wrist-worn). The RespiBAN device recorded ECG, EMG, EDA, and TEMP at a sampling rate of 700 Hz. Meanwhile, the Empatica E4 wristband collected BVP at 64 Hz, along with EDA and TEMP at 4 Hz, and 3-axis ACC at 32 Hz [41]. Participants were exposed to four distinct mental states: baseline (non-stressed), amusement, stress (induced by the Trier social stress test involving public speaking), and meditation (aimed at promoting relaxation and returning participants to a neutral affective state) [41]. In this study, we specifically utilized BVP signals for stress detection. Table II provides a detailed description of the WESAD dataset, focusing on the BVP signal.

TABLE II  
SUMMARY OF THE DEMOGRAPHIC INFORMATION FOR BVP SIGNAL IN WESAD DATASET

Item	Information
Subjects	15
Gender (M/F)	12 Male & 3 Female
Age (mean $\pm$ SD)	27.5 $\pm$ 2.4
Trials per subject	2
Total trials	30
Total duration	450 minutes (approx..)
Sampling frequency	64Hz (BVP)

\*Standard Deviation (SD)

## B. Signal Pre-Processing

This subsection provides an overview of data segmentation, normalization, and data augmentation.

### 1) Data Segmentation and Normalization:

The data were segmented into 30-second non-overlapping windows and paired with their corresponding labels. To ensure the signal amplitudes remained within a specific range, BVP signals were z-score normalized [16], [40]. Fig. 2 illustrates a segment of the BVP signal before and after normalization.

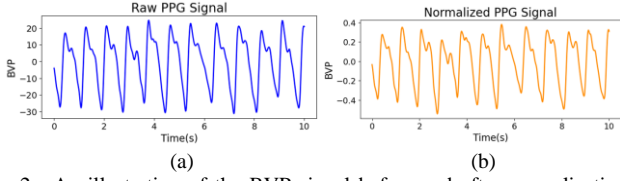


Fig. 2. An illustration of the BVP signal before and after normalization is presented. Initially, the raw BVP signal (a) ranges between -30 and 20. After normalization (b), the signal range is adjusted to approximately -0.4 to 0.4. This normalization process standardizes the signal, facilitating more consistent and accurate analysis.

## 2) Data Augmentation:

The RUET SPML dataset has more stress recordings, while the WESAD dataset has a larger baseline class, leading to class imbalances that affect both datasets. Such imbalances make it challenging to train deep learning models for stress monitoring, as the models must effectively capture complex non-linear patterns while avoiding overfitting due to limited training data [40], [49]. To address this, data augmentation was applied during training.

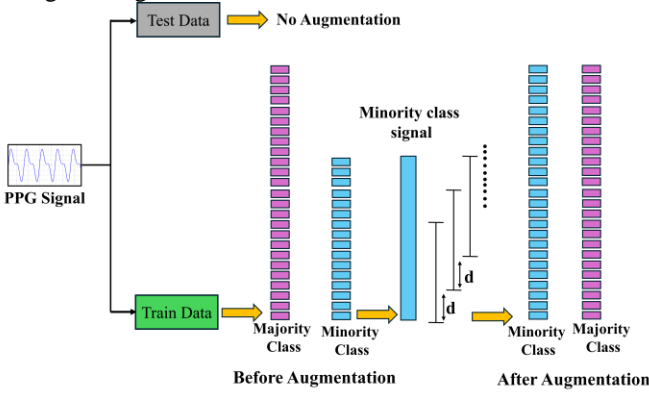


Fig. 3. An illustration of the data augmentation process. The training data was augmented to mitigate class imbalance, particularly to enhance the representation of the minority class. This process involved generating samples by modifying existing ones within the minority class to improve its distribution in the dataset.

We adopted a simple sliding window-based method to augment the minority class. Initially, a non-overlapping 30-second windows were used to extract segments from the minority class. The number of data points and samples in both majority and minority classes were then calculated to ensure the generation of an equal number of samples for the minority class. Subsequently, the minority class windows were merged to form a continuous signal, from which augmented segments were generated. The difference between two successive start or end indices of the data points, i.e., step size  $d$  was determined using equation (1). The augmentation process is explained in Algorithm 1 and Fig. 3.

$$d = \frac{(t_{minority} - t_{window}) \times F_s}{n_{majority} - 1} \quad (1)$$

where,

$t_{minority}$  = time length of minority class

$t_{window}$  = time length default window

$F_s$  = sampling frequency of the signal

$n_{majority}$  = number of samples of majority class

**Algorithm 1:** Generation of augmented minority class segments using a 30-second sliding overlapping window technique, ensuring an equal number of samples between the minority and majority classes to address data imbalance effectively.

### Data:

- A dataframe containing the minority class with desired window length.
- Parameters: desired window ( $t_{window}$  in sec), sampling frequency of the signal ( $F_s$  in Hz), number of augmented samples to generate for balancing

### Result:

Augmented minority class training set with  $n_{majority}$  samples.

### Data Augment:

#### Start

- 1 Reshape the minority class windowed data frame to signal, i.e., the whole signal into a single row, and compute the step size (d) between two windows from equation (1).
- 2 Initialize start\_index = 0 and end\_index =  $t_{window} \times F_s$ .
- 3 Generate augmented samples:
  - a) Extract segment from reshaped data and append to augmented dataframe.
  - b) Update indices:
    - start\_index = start\_index + d
    - end\_index = end\_index + d
- 4 Append minority class labels to all rows of the augmented dataframe.
- 5 Return augmented dataframe.

#### End

## C. Transpose-Enhanced Autoencoder Network (TEANet)

For stress detection, the proposed transpose-enhanced autoencoder network architecture, demonstrated in Fig. 4, consists of an input layer connected to a down-sampling block, followed by transpose-enhanced autoencoder layers and classification blocks with a view to extracting various features from the BVP signals. The transpose-enhanced autoencoder (TEA) layer comprises two parallel paths: the transpose-enhanced (TE) path and the convolutional path. The transpose-enhanced path incorporates a transposed convolutional block, convolutional blocks, and autoencoder blocks, whereas the convolutional path comprises two convolutional blocks. The outputs of these paths are concatenated and forwarded to the classification blocks, thus passed to the classification stage. Let, the feature map from the dataset be  $X \in \mathbb{R}^{N \times d}$  and each sample  $x_i \in X$ , where,  $x_i = \{x_1, x_2, x_3, \dots, x_N\}$ , and  $N$  represents the total number of samples, and  $d$  represents data points. However, detailed descriptions of the structure and functionality of each block are provided below.

### 1) Down-sampling Block (DSB)

This block consists of a Conv1D layer with 128 filters, a kernel size of 5, and a stride of 4, followed by MaxPooling1D with a pool size of 2, stride of 2, batch normalization, and ReLU activation. This block reduces the input length to one-eighth in two steps: one-fourth via Conv1D and half via MaxPooling1D, which reduces the complexity in the subsequent layers. It also extracts key features in the initial stages, making it an essential component for efficient feature representation. Mathematically the outputs from the Conv1D layer,

$$z_i[j] = \sum_{t=0}^{k-1} w[t] * x_i[j+t] + b \quad (2)$$

where,  $j = 1, 2, 3, \dots, \frac{d-k}{s} + 1$ ,  $k$  = filter size,  $s$  = strides,  $w$  = weights,  $b$  = biases.

The output from the MaxPooling1D layer,

$$z_i^{pool}[j] = \max\{z_i[j \cdot s_p], z_i[j \cdot (s_p + 1)], \dots, z_i[j \cdot s_p + p - 1]\} \quad (3)$$

where,  $s_p$  = strides,  $p$  = pool size.

The output from the BatchNormalization layer,

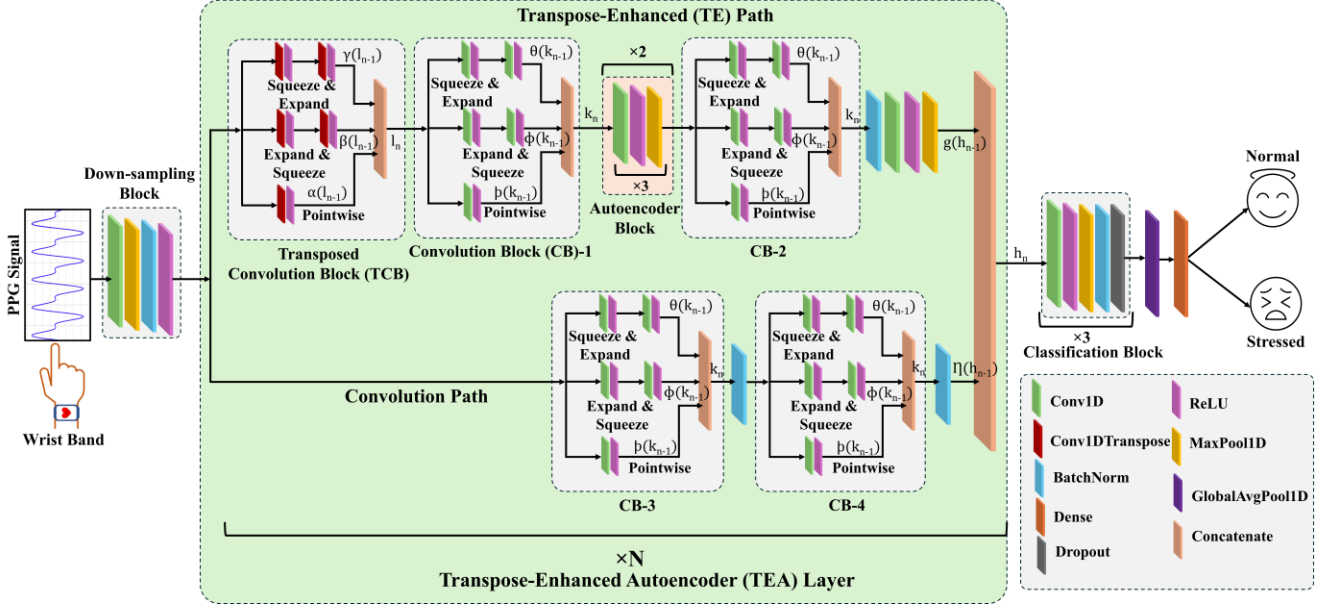


Fig. 4. The detailed architectural framework of the transpose-enhanced autoencoder network (TEANet): a novel approach for addressing class imbalance and enhancing robustness in BVP-based stress detection for wearable devices.

$$\hat{z}_i[j] = \frac{z_j^{pool}[j] - \mu_j}{\sqrt{\sigma_j^2 + \varepsilon}} \quad (4)$$

where,  $\mu_j$  = mean,  $\sigma_j$  = standard deviation,  $\varepsilon$  = a small positive number to prevent division by zero. After applying learnable parameters  $\delta$  (scale) and  $\Delta$  (shift),

$$\tilde{z}_i[j] = \delta \cdot \hat{z}_i[j] + \Delta \quad (5)$$

the ReLU introduces nonlinearity followed by the equation (6).

$$o_i[j] = \max(0, \tilde{z}_i[j]) \quad (6)$$

The output,  $o_i[j]$  then fed to the TEA layer.

## 2) Transpose-Enhanced Autoencoder (TEA) Layer

The TEA layer consists of fundamental building blocks namely convolutional block (CB), transpose convolutional block (TCB), and autoencoder block. The fundamental blocks are detailed below.

### a) Convolutional Block (CB)

The convolutional block comprises three distinct paths, each contributing uniquely to feature-extraction and transformation. The pointwise path  $b(\cdot)$ , consisting of a single Conv1D layer with a kernel size of 1 followed by ReLU activation, plays a crucial role in transforming input features into a new feature space by focusing on inter-channel dependencies. In contrast, the expand-and-squeeze path  $\phi(\cdot)$  and squeeze-and-expand path  $\theta(\cdot)$  utilize Conv1D layers with kernel sizes of 9 and 3, respectively, each followed by ReLU activation. The expansion step

enhances the receptive field, capturing broader contextual information, while the squeezing step refines the feature representation by focusing on local patterns. At the end of this block, the outputs from all three paths are concatenated, effectively combining diverse feature representations to enrich the input for subsequent layers. The features  $k_{n-1}$  from the previous block are processed to provide the output  $k_n$  as described in equation (7).

$$k_n = \text{concatenate}[\theta(k_{n-1}), \phi(k_{n-1}), b(k_{n-1})] \quad (7)$$

### b) Transpose Convolutional Block (TCB)

This block is designed similarly to the convolutional clock, with the primary distinction being the replacement of the Conv1D layer by the Conv1DTranspose layer. The pointwise transpose convolution operation  $\alpha(\cdot)$  applies learnable weights to perform a feature-space transformation without altering the temporal resolution of the input. In contrast, the expand-and-squeeze path  $\beta(\cdot)$  captures broader temporal patterns, while the squeeze-and-expand  $\gamma(\cdot)$  path focuses on local patterns of the input features. The hierarchical features extracted from these three paths are aggregated using a concatenate layer. This block enhances high-level feature representations by enabling the model to reconstruct information from compressed feature maps. It ensures the recovery of fine-grained details that may have been lost during the down-sampling process in earlier

TABLE III  
THE NUMBER OF FILTERS IN THE TRANSPOSE-ENHANCED AUTOENCODER (TEA) LAYERS

Block	Transposed Conv Block			Conv Block-1			Conv Block-2			Conv Block-3			Conv Block-4		
	$f_p$	$f_{ese}$	$f_{ses}$	$f_p$	$f_{ese}$	$f_{ses}$	$f_p$	$f_{ese}$	$f_{ses}$	$f_p$	$f_{ese}$	$f_{ses}$	$f_p$	$f_{ese}$	$f_{ses}$
1	64	64	16	16	32	64	16	32	32	16	32	96	16	96	96
2	32	32	16	16	32	64	16	96	96	16	96	96	16	64	64
3	64	64	32	16	32	64	16	96	96	16	16	32	16	64	64
4	64	64	16	16	32	96	16	16	32	16	32	64	16	96	96
5	64	64	96	64	16	16	16	32	32	16	64	64	64	96	96
6	64	64	96	64	16	16	16	32	32	16	64	64	64	96	96
7	64	64	96	64	16	16	16	32	32	16	64	64	64	96	96

TEA layers, especially when multiple TEA layers are employed. Furthermore, the multi-scale reconstructions provided by this block enhance robustness in handling complex input patterns, such as those encountered in stress monitoring tasks. The input features from the previous block,  $l_{n-1}$ , are processed to compute the output  $l_n$ , as outlined in Equation (8).

$$l_n = \text{concatenate}[\alpha(l_{n-1}), \beta(l_{n-1}), \gamma(l_{n-1})] \quad (8)$$

c) **Autoencoder Block (AB)**

The autoencoder block is used for feature extraction through convolution operations. It consists of three Conv1D layers, each followed by MaxPooling1D with a pool size of 2. The convolutional layers have kernel sizes of 3 and filters of 96, 16, and 32, respectively. This block down-samples the features while emphasizing important ones, enhancing the model's ability to capture key patterns.

The blocks described above are the building blocks for the TEA layer. As earlier described, this layer comprises two main components including the convolutional path  $\eta(\cdot)$ , and the transpose-enhanced (TE) path  $g(\cdot)$ . These components work together to extract and transform features, with the Convolutional path capturing local and global patterns, while the TE path reconstructs important features. The outputs from both paths are then concatenated and passed to the classification blocks for final processing. The descriptions of two paths are detailed below

i. **Convolutional Path,  $\eta(\cdot)$**

The convolutional path consists of two convolutional blocks each followed by batch normalization, designed to extract and refine features through successive convolutional operations. These blocks leverage multiple Conv1D layers with varying kernel sizes and ReLU activations to capture both local and global patterns in the input data. By combining these blocks, the Convolutional Path effectively enhances the feature representation, providing richer inputs for the subsequent layers of the model.

ii. **Transpose-Enhanced (TE) Path,  $g(\cdot)$**

The transpose-enhanced path consists of a transpose-enhanced block, several convolutional blocks, and two autoencoder blocks. The transposed convolutional block reconstructs key features from previous layers, which are then passed through a convolutional path. This path propagates the features through an autoencoder block, followed by a convolutional block, batch normalization, another Conv1D layer for shape matching with kernel size 1, and a ReLU activation. Finally, the features are downsampled with a MaxPooling1D layer (pool size 2). This path effectively reconstructs and refines important features for subsequent

processing. If the previous features are represented as  $h_{n-1}$ , then the output,

$$h_n = \text{concatenate}[\eta(h_{n-1}), g(h_{n-1})] \quad (9)$$

The output  $h_n$  from the TEA layer is then fed to the classification block for further processing.

3) **Classification Block**

The classification block consists of Conv1D, ReLU, MaxPooling1D, Batch Normalization, and Dropout layers, with a pool size of 2 and a dropout rate of 0.3. This block is repeated three times, with the number of filters changing from 96 to 64, and then to 32. Afterward, a global average pooling layer processes the concatenated output, and the final prediction is generated by a dense layer with a softmax activation function, described as:  $\text{softmax}(\mathbf{x}) = \frac{e^{x_i}}{\sum_{j=1}^n e^{x_j}}$  (10)

To facilitate a comparison of the performance of the proposed architecture, we evaluate configurations with two to seven layers. The filter numbers used in the TEA Layers, which have not been previously specified, are detailed in Table III for clarity and reference. The numbers of filters are denoted by  $f_p$ ,  $f_{ese}$ ,  $f_{ess}$ ,  $f_{ses}$ ,  $f_{see}$ , representing the number of filters in the pointwise layer, expand layer of the expand-and-squeeze path, squeeze layer of the expand-and-squeeze path, squeeze layer of the squeeze-and-expand path, and expand layer of the squeeze-and-expand path, respectively. We have chosen  $f_p = f_{ese} = f_{ess}$ .

Root Mean Square Propagation (RMSprop) is an optimization algorithm designed to handle the challenges of training deep neural networks [50], particularly dealing with the problem of vanishing, and exploding gradients by adapting the learning rate based on recent gradients, was used as the optimizer. It computes the exponentially weighted moving average of the squared gradients as the equation (11),

$$E[g^2]_t = \gamma E[g^2]_{t-1} + (1 - \gamma)g_t^2 \quad (11)$$

where  $\gamma$  is the decay rate,  $g$  represents the gradient.

And updates the parameters as defined by the equation (12).

$$\theta_{t+1} = \theta_t - \frac{\rho}{\sqrt{E[g^2]_t + \epsilon}} g_t \quad (12)$$

where  $\theta$  is the learnable parameters,  $\rho$  is the learning rate, and  $\epsilon$  is a small constant to prevent division by zero.

In this study, a sparse categorical cross-entropy loss function was used, which is often applied in multi-class classification tasks but can also be used for binary classification, measures the difference between two probability distributions: predicted probabilities  $\hat{y}$  and actual labels  $y$ . This loss function  $L(y, \hat{y})$ , described by Equation (13), was employed to calculate the loss during training.

$$L(y, \hat{y}) = -\sum_{c=0}^1 y_c \log(\hat{y}_c) \quad (13)$$

It is particularly suitable for binary classification tasks,

TABLE IV  
PERFORMANCE COMPARISON OF THE TRANSPOSE-ENHANCED AUTOENCODER NETWORK WITH VARYING NUMBERS OF TEA LAYERS. THE BEST RESULTS ARE HIGHLIGHTED IN BOLD.

Dataset	RUET SPML						WESAD					
	Acc	Spe	Sen	F1	AUC	k	Acc	Spe	Sen	F1	AUC	k
TEA-7 Layers	91.20	83.33	93.84	94.04	0.8925	0.7672	95.84	96.03	95.40	94.34	0.9814	0.9105
TEA-6 Layers	91.19	<b>84.21</b>	93.55	94.02	0.9131	0.7667	96.29	96.55	95.71	95.03	0.9807	0.9208
TEA-5 Layers	<b>92.51</b>	82.46	95.89	<b>95.03</b>	<b>0.9261</b>	<b>0.7915</b>	95.85	96.37	94.79	94.46	0.9803	0.9114
TEA-4 Layers	91.18	81.58	94.43	94.08	0.9166	0.7621	96.58	97.06	95.71	94.92	<b>0.9849</b>	0.9239
TEA-3 Layers	92.08	83.33	95.01	94.71	0.9300	0.7824	<b>96.94</b>	<b>97.06</b>	<b>96.63</b>	<b>95.95</b>	0.9824	<b>0.9350</b>
TEA-2 Layers	92.07	83.33	<b>95.01</b>	94.79	0.9190	0.7697	95.09	94.30	96.32	93.89	0.9751	0.8984

helping the model to differentiate between the two classes more effectively.

D. Performance Metrics

We have evaluated several indices for stress classification (normal versus stressed) performance measurement of the TEANet including accuracy, sensitivity, specificity, F1-score, area under the curve (AUC) and Cohen’s kappa coefficient (k). To rigorously evaluate the proposed model, this study employed leave-one-subject-out (LOSO) cross-validation. In this method, one subject is reserved for testing, while the model is trained in the remaining subjects. This iterative process ensures that each subject is used as a test case exactly once, providing a comprehensive assessment of the model’s generalizability and performance across diverse individuals.

III. RESULTS AND DISCUSSION

The performance of TEANet was evaluated across varying TEA layers, denoted as TEA-N layers, ranging from TEA-2 to TEA-7, where N represents the number of TEA layers. As shown in Table IV. The model achieves the highest overall performance on the RUET SPML dataset with TEA-5 layers, while TEA-6 layers demonstrated the highest specificity of 84.21%, indicating improved accuracy for the minority class. In contrast, TEANet performed best on the WESAD dataset with TEA-3 layers. Based on these findings, TEANet with TEA-6 layers for the RUET SPML dataset and TEA-3 layers for the WESAD dataset were selected for detailed analysis. The proposed model demonstrates remarkable performances, achieving 92.19% accuracy, 84.21% specificity, 93.55% sensitivity, 94.02% F1-score, 0.9131 AUC, and 0.7667 kappa with the RUET SPML dataset. On the other hand, 96.93% accuracy, 97.06% specificity, 96.63% sensitivity, 95.95% F1-score, 0.9824 AUC, and 0.9350 kappa score with the WESAD dataset. Fig. 5 highlights the variations in performance across subjects for both datasets. The results underscore the model’s outstanding capability to distinguish between normal and stressed classes.

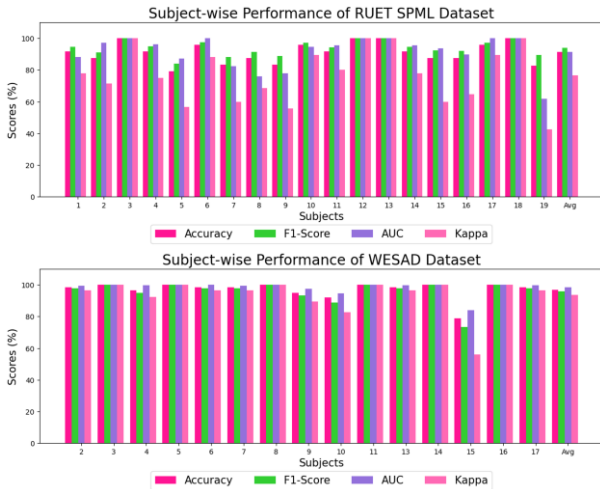


Fig. 5. Subject-wise performances including accuracy in %, F1-score in %, AUC, and Cohen’s k values of, RUET SPML dataset with TEA-6 layers (top) and WESAD dataset with TEA-3 layers (bottom).

Moreover, the performance across TEA-2 to TEA-7 layers shows minimal deviation, highlighting the scalability and

optimization potential of TEANet, making it a promising solution for stress detection in diverse real-world scenarios.

A. Effect of Augmentation

TABLE V  
PERFORMANCES OF THE TEANET WITH AND WITHOUT AUGMENTATION TO STUDY THE EFFECT OF AUGMENTATION.

Dataset	Data Aug	Acc	Spe	Sen	F1	AUC	k
RUET SPML	No	88.76	71.05	<b>94.72</b>	92.85	0.8636	0.6567
	Yes	<b>91.19</b>	<b>84.21</b>	93.55	<b>94.02</b>	<b>0.9131</b>	<b>0.7667</b>
WESAD	No	93.89	95.51	90.80	91.40	0.9669	0.8682
	Yes	<b>96.94</b>	<b>97.06</b>	<b>96.63</b>	<b>95.59</b>	<b>0.9824</b>	<b>0.9350</b>

Data augmentation was applied during training to reduce the model bias toward the majority class, effectively decreasing the likelihood of overfitting [51]. The effect of data augmentation on the model performance is demonstrated in Table V. For the RUET SPML dataset, data augmentation improves accuracy by 2.43%, specificity by 13.16%, F1-score by 1.17%, AUC by 4.95%, and kappa by 11%, while slightly reducing sensitivity by 1.17%. Whereas, for the WESAD dataset, data augmentation enhances accuracy by 3.05%, specificity by 1.55%, sensitivity by 5.83%, F1-score by 4.55%, AUC by 1.55%, and kappa by 6.68%. Although sensitivity decreases by 1.17% in the RUET SPML dataset, the overall performance, particularly for the minority class, improves significantly due to the data augmentation.

Fig. 6 presents the confusion matrices for different cases, where Figs 6(a) and 6(b) illustrate the improvement in the minority class for the RUET SPML dataset without and with augmentation, while Figs 6(c) and 6(d) show the performance for the WESAD dataset. These results underscore the effectiveness of data augmentation in improving minority class accuracy i.e., specificity in RUET SPML dataset, and sensitivity in WESAD dataset, leading to a more balanced overall performance.

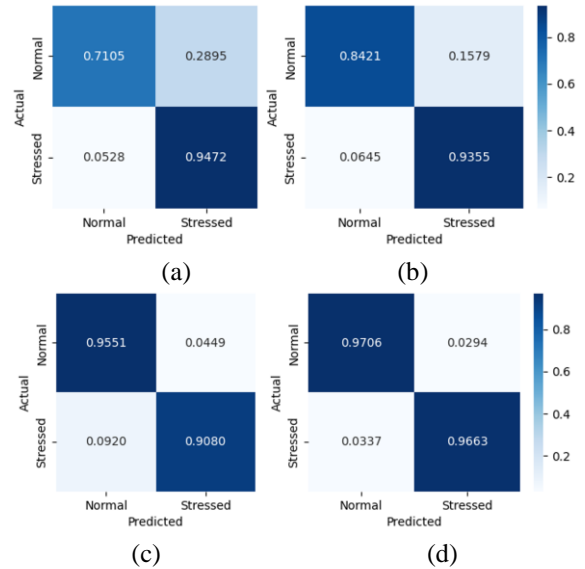


Fig. 6. Normalized confusion matrices for the RUET SPML dataset (a) without augmentation, (b) with augmentation. Normalized confusion matrices for the WESAD dataset (c) without augmentation, (d) with augmentation. The confusion matrices clearly demonstrate significant improvement following data augmentation during training on both datasets.

TABLE VI  
THE COMPARISON OF PERFORMANCES WITH THE DIFFERENT VARIANTS OF THE PROPOSED ARCHITECTURE AND THE SELECTION PROCESS OF THE TEANET. THE BEST RESULTS ARE HIGHLIGHTED IN BOLD.

Dataset	RUET SPML						WESAD					
	Model	Acc	Spe	Sen	F1	AUC	k	Acc	Spe	Sen	F1	AUC
TE Path without TCB	86.57	59.65	95.60	91.62	0.8441	0.5650	94.41	95.85	91.72	91.49	0.9644	0.8770
TE Path without Autoen.	88.76	63.16	97.36	93.40	0.7984	0.6339	95.94	98.45	91.41	93.40	0.9788	0.9062
TE Path	87.66	67.54	94.43	92.06	0.8390	0.6290	94.75	94.30	95.40	93.18	0.9721	0.8895
Conv Path	91.39	75.44	96.77	<b>94.51</b>	0.9105	0.7387	95.31	95.85	94.17	93.39	0.9738	0.8981
TEANet	<b>91.19</b>	<b>84.21</b>	<b>93.55</b>	94.02	<b>0.9131</b>	<b>0.7667</b>	<b>96.94</b>	<b>96.06</b>	<b>95.63</b>	<b>95.95</b>	<b>0.9824</b>	<b>0.9350</b>

### B. Ablation Study

Our proposed TEA layer comprises two components: the TE path and the convolutional path. The TE path includes a TCB, CB, autoencoder block, and supporting layers. To evaluate their contributions, an ablation study was done considering four TEANet variants:

1. TE path without TCB
2. TE path without autoencoder
3. TE path only
4. Convolutional path only

The TE path without the TCB module showed biased performance towards majority class on both datasets, predicting the minority class (i.e., specificity) of 59.6% for RUET SPML and 91.7% (sensitivity) for WESAD. Excluding the autoencoder module, i.e., utilizing the TE path without the autoencoder, improves overall accuracy, particularly with the RUET SPML dataset. However, it offers limited performance on the minority class for both datasets, which remains our primary focus. On the RUET SPML dataset, specificity was 67.5%, while on WESAD, sensitivity was 95.4%. Comparatively, the full TE path achieved minority class accuracies of 63.2% (RUET SPML) and 91.4% (WESAD). These results demonstrate the autoencoder's role in mitigating class imbalance. The convolutional path alone outperformed individual TE path variants, achieving 75.4% and 94.2% accuracies for the minority class in RUET SPML and WESAD datasets, respectively. However, neither path independently achieved balanced performance. The combined paths, the full TEANet architecture, delivered more consistent results for both the datasets. The results of the ablation study are shown in Table VI.

In summary, the inclusion of the autoencoder module and the integration of TEA and convolutional paths i.e., the complete TEANet were essential for addressing class imbalance. This

study underscores the effectiveness of the proposed architecture in handling imbalanced datasets, particularly the challenging RUET SPML dataset.

### C. Comparison with State-of-the-Art Architecture

To assess the efficiency of our proposed TEANet model, a comparative analysis with established convolutional and transformer-based architectures was performed. The performance of our model was compared with AlexNet, MobileNet-V1, and ResNet-18 from convolutional models, as well as CNN with transformer (CNN+TF) and multi-perspective channel-attention with transformer (MPCA+TF) [52] from transformer-based models.

Among convolutional architectures, ResNet-18 outperformed conventional models but struggled with identifying the minority class, achieving an accuracy of 71.1% for the minority class in the RUET SPML dataset. Likewise, among transformer-based architectures, CNN+TF outperformed MPCA+TF; however, both methods failed to effectively address class imbalance, resulting in suboptimal overall performance. Compared to these state-of-the-art architectures, TEANet not only demonstrated superior overall performance but also achieved substantial improvements in minority class classification, with increases of 13.16% and 32.46% over the best-performing convolutional and transformer-based models, respectively. These findings highlight TEANet's ability to maintain balanced performance, particularly in handling class-imbalanced datasets, while achieving high overall classification accuracy.

### D. Comparative Analysis with the State-of-the-Art Models for Stress Monitoring Using Wearable Device

A comparative analysis of our work with existing BVP-based stress classification studies is summarized in Table VIII. This comparative analysis serves to contextualize our contributions within the broader field and highlight the novel aspects of our

TABLE VII  
PERFORMANCE COMPARISON OF THE TRANSPOSE-ENHANCED AUTOENCODER NETWORK WITH STATE-OF-THE-ART ARCHITECTURE. THE BEST RESULTS ARE HIGHLIGHTED IN BOLD.

Type	Model	Dataset											
		RUET SPML						WESAD					
		Acc	Spe	Sen	F1	AUC	k	Acc	Spe	Sen	F1	AUC	k
Convolutional	AlexNet	81.96	42.11	95.31	88.96	0.6425	0.3874	94.53	<b>96.37</b>	91.10	91.77	0.9580	0.8778
	MobileNet-V1	80.43	29.82	97.36	88.32	0.6465	0.2919	95.59	95.51	95.71	93.62	0.9748	0.9032
	ResNet-18	90.07	71.05	96.48	93.74	0.8673	0.6901	96.71	95.68	<b>98.47</b>	95.84	0.9872	0.9315
Transformer	CNN+TF	85.03	51.75	96.19	90.83	0.7611	0.4822	92.52	95.51	87.12	88.58	0.9329	0.8314
	MPCA+TF	78.23	13.16	<b>100.00</b>	87.53	0.5103	0.1368	95.31	95.68	94.48	93.68	0.9634	0.9001
This Work	TEANet	<b>91.19</b>	<b>84.21</b>	93.55	<b>94.02</b>	<b>0.9131</b>	<b>0.7667</b>	<b>96.94</b>	96.06	96.63	<b>95.95</b>	<b>0.9824</b>	<b>0.9350</b>



proposed approach. The comparative analysis presented in Table VIII reveals that our proposed method outperforms the majority of existing BVP-based stress classification studies, with notable exceptions being studies [8], [26], and [28]. A common characteristic of many previous works, including [8], [26], and [28], is their reliance on feature engineering techniques. Studies [8], [28], and [53] further complicate its methodology by incorporating multiple physiological signals and relying on manual feature extraction in traditional machine learning approaches. While the study [26] utilizes only BVP signals, it introduces a complex peak detection and denoising process followed by traditional ML classifiers. In contrast, our method achieves competitive performance by directly processing raw BVP signals without the need for intricate preprocessing or handcrafted features. This streamlined approach enhances the practical applicability and generalizability of our model.

TABLE VIII  
THE COMPARATIVE ANALYSIS OF OUR WORK WITH THE EXISTING LITERATURES  
FOCUSING ON STRESS MONITORING

Ref.	Dataset	Signals	Method	Acc.
Alshamrani [38]	WESAD	BVP, ACC, TEMP	FCN	85%
Bellante <i>et al.</i> [28]	WESAD	BVP, EDA, RESP	SVM	97.2%
Bobade <i>et al.</i> [8]	WESAD	ACC, ECG, BVP, EDA, EMG, RESP	ANN	95.21%
Benchekroun <i>et al.</i> [24]	Private	PPG	RF	83%
Rashid <i>et al.</i> [36]	WESAD	PPG	H-CNN	88.56%
Zhu <i>et al.</i> [29]	WESAD	EDA	SVM	83.9%
Schmidt <i>et al.</i> [41]	WESAD	BVP	LDA	85.83%
Heo <i>et al.</i> [26]	WESAD	PPG	LDA	96.5%
Jahanjoo <i>et al.</i> [53]	WESAD	PPG	SVM	95.55%
Kalra <i>et al.</i> [35]	Private	PPG	DNN	90.5%
<b>This work</b>	RUET SPML	<b>BVP</b>	<b>TEANet</b>	<b>92.5%</b>
<b>This work</b>	WESAD	<b>BVP</b>	<b>TEANet</b>	<b>96.9%</b>

The proposed TEANet model excels in stress classification. The study [8] reports 95.21% accuracy, but with a large number of multimodal signals; on the other hand, Heo *et al.* [26] achieved 96.5% accuracy with LDA, but with a larger window length of 120 seconds. Additionally, Jahanjoo *et al.* [53] achieve a good accuracy of 95.55% with a larger window size, and Bellante *et al.* [28] report better performance than ours, but also with larger windows and a larger number of signals, unlike ours, which relies solely on BVP. A thorough comparison with existing methods emphasizes the innovative approach and enhanced performance of TEANet, establishing it as a highly effective solution for real-world stress monitoring, particularly in wearable technology applications.

E. Interpretability of the Proposed Model

The interpretability of the proposed TEANet model is illustrated through feature visualization using uniform manifold approximation and projection (UMAP) [54] technique, as shown in Fig. 7. The figure provides a two-dimensional representation of the features as they progress through various layers of the model during the learning process.

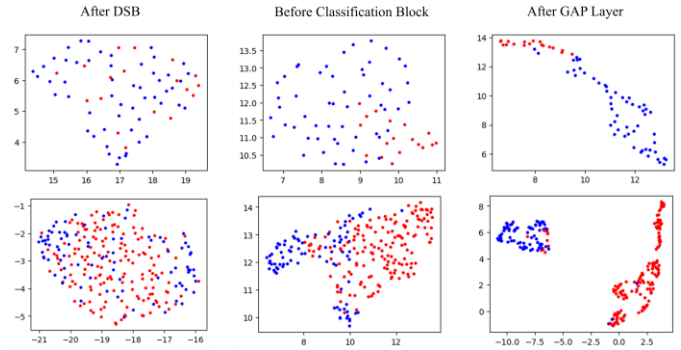


Fig. 7. Feature visualization of various layers illustrating the learning process of the TEANet model using uniform manifold approximation and projection. The top row depicts feature representations from the RUET SPML dataset, while the bottom row shows feature representations from the WESAD dataset. These visualizations highlight the effective class separation between the normal (red) and stressed (blue) classes.

The top and bottom row represent the feature visualization of the RUET SPML (top), and WESAD dataset (bottom) respectively. The red dots represent the features of the normal class, while the blue dots represent the features of the stressed class. The first column represents the feature visualization after the classification block in the TEANet. In this stage, the features of both normal (blue) and stressed (red dots) classes samples are indistinguishable, indicating that the initial stage lack clear separation of the features. The second column illustrates the features after the TEA layer (before the classification block). In this stage, as the features pass through the subsequent blocks (number of layers), the model extracts significant patterns from the signal, leading to a gradual improvement in the separability. Lastly, the third column represents the feature representation of the 1D global average pooling layer of both datasets. The clear distinction in the feature space at this stage underscores the effectiveness of the model in capturing complex patterns and dependencies within the data. This progressive enhancement in feature separability across layers demonstrates the model's capacity to learn meaningful representations, ultimately contributing to its robust classification performance. This visualization conveys the model's ability to refine and distinguish data as it delves deeper into the model, providing a clear and interpretable explanation of the decision-making process within the TEANet.

F. Explainability of the Proposed Model Using Feature Maps

Deep learning models are often perceived as black boxes, limiting their applicability in critical domains due to a lack of explainability [55]. Feature maps provide a valuable means to address this challenge by offering insights into the model's decision-making process. Fig. 8 depicts the feature maps of signals processed by the proposed model, emphasizing the regions of the signal that the model identifies as most significant for its decisions. The feature maps were extracted from the last convolutional layer, which contains 32 filters. The teal-colored feature maps (left) represent normal samples, while the purple-colored feature maps (right) correspond to stressed samples of the BVP signals. The distinct activation patterns observed between the normal and stressed classes demonstrate the model's capacity to differentiate effectively between these states, underscoring its ability to identify critical features for decision-making process.

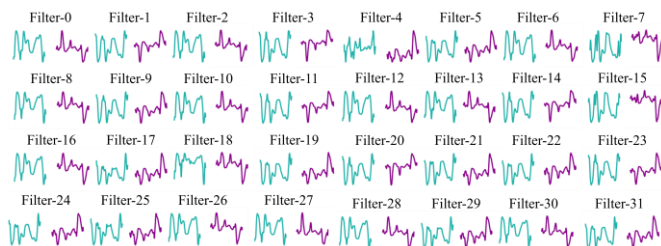


Fig. 8. Feature map of the last convolution layer of the classification block having 32 filters for normal (left) and stressed (right) of each filter on the RUET SPML dataset capturing different patterns of the BVP signal. The teal color represents normal class samples, and the magenta color represents the stressed class samples respectively.

### G. Wearable Devices Compatibility

Heart activity, reflected by blood volume changes, can be measured using photoplethysmography sensors, with BVP signals containing valuable information related to stress [22], [23]. Therefore, analyzing BVP signals can facilitate stress detection. Extracting this information using traditional feature-engineered methods is often inadequate, as important features may be discarded, whereas deep learning models, capable of handling both raw data and extracted features, have become the leading approach for pattern recognition tasks [40]. Moreover, BVP signals can be collected conveniently, and many commercially available wearable devices are equipped with these sensors due to their affordability [17], [56]. The growing demand for continuous stress monitoring among health-conscious individuals is rising, as mental stress can lead to various health complications [57]. Therefore, commercially available smart wearable devices offer opportunities for automatic stress monitoring in everyday settings. Manufacturers are interested in embedding sensors like BVP due to their affordability and ease of use. In this study, we investigated automatic stress monitoring using the transpose-enhanced autoencoder network, a deep neural network model, to classify emotional stress levels as either normal or stressed using BVP signals. It exhibited state-of-the-art performance on the publicly available WESAD dataset and the self-collected RUET SPML dataset, outperforming existing approaches. This suggests its potential for integration into commercially available smart wearables, offering a promising pathway for automatic stress monitoring in everyday settings.

## IV. CONCLUSION

This study introduces a novel model, TEANet, for automated stress monitoring using wearable BVP signals. Given the non-invasive nature and widespread availability of BVP sensors, the proposed model effectively addresses the critical need for efficient stress assessment in resource-constrained environments using BVP signals. The model's performance was comprehensively evaluated across diverse datasets, demonstrating superior results compared to existing state-of-the-art methods. This paper highlights the model's robustness, achieving a highest accuracy of 92.51% and an F1 score of 95.03% using the RUET SPML dataset, and a highest accuracy of 96.94% and an F1 score of 95.95% for stress detection using the WESAD dataset, evaluated through leave-one-subject-out cross-validation. This validation approach underscores the model's generalizability for real-world applications. A key

contribution to this work is its demonstration of superior stress monitoring performance using only a single BVP signal, which is typically considered less informative for stress analysis. This underscores the robustness and practicality of the model, particularly given the ease of acquiring BVP signals in wearable devices. Moreover, UMAP-based feature visualization across different layers is utilized, offering insights into the model's decision-making process and improving interpretability. In conclusion, this study presents a highly accurate and efficient deep-learning model for stress monitoring using a single, readily available BVP signal. The findings indicate significant potential for practical implementation in wearable devices, facilitating continuous and non-invasive stress monitoring. Future work will explore multi-class stress level classification, incorporate additional physiological signals, smaller window size, hardware implementation, and investigate the model's performance in stress detection scenarios to further enhance its applicability in real-world settings.

## ACKNOWLEDGMENT

This manuscript is currently under review and has been submitted to the *IEEE Journal of Biomedical and Health Informatics*. This version is a pre-print and may be subject to changes in the final published version.

## REFERENCES

- [1] H. Haykin and A. Rolls, "The neuroimmune response during stress: A physiological perspective," *Immunity*, vol. 54, no. 9, pp. 1933-1947, 2021.
- [2] B. S. McEwen *et al.*, "Mechanisms of stress in the brain," *Nature neuroscience*, vol. 18, no. 10, pp. 1353-1363, 2015.
- [3] J. K. Rout, K.-K. R. Choo, A. K. Dash, S. Bakshi, S. K. Jena, and K. L. Williams, "A model for sentiment and emotion analysis of unstructured social media text," *Electronic Commerce Research*, vol. 18, pp. 181-199, 2018.
- [4] M. Krommyda, A. Rigos, K. Bouklas, and A. Amditis, "An experimental analysis of data annotation methodologies for emotion detection in short text posted on social media," in *Informatics*, 2021, vol. 8, no. 1: MDPI, p. 19.
- [5] H. Kaya, F. Gürpınar, and A. A. Salah, "Video-based emotion recognition in the wild using deep transfer learning and score fusion," *Image and Vision Computing*, vol. 65, pp. 66-75, 2017.
- [6] P. Zhang *et al.*, "Real-time psychological stress detection according to ECG using deep learning," *Applied Sciences*, vol. 11, no. 9, p. 3838, 2021.
- [7] J. Henry, H. Lloyd, M. Turner, and C. Kendrick, "On the robustness of machine learning models for stress and anxiety recognition from heart activity signals," *IEEE Sensors Journal*, vol. 23, no. 13, pp. 14428-14436, 2023.
- [8] P. Bobade and M. Vani, "Stress detection with machine learning and deep learning using multimodal physiological data," in *2020 Second International Conference on Inventive Research in Computing Applications (ICIRCA)*, 2020: IEEE, pp. 51-57.
- [9] F. Albertetti, A. Simalastar, and A. Rizzotti-Kaddouri, "Stress detection with deep learning approaches using physiological signals," in *International Conference on IoT Technologies for HealthCare*, 2020: Springer, pp. 95-111.
- [10] O. M. Mozos *et al.*, "Stress detection using wearable physiological and sociometric sensors," *International journal of neural systems*, vol. 27, no. 02, p. 1650041, 2017.
- [11] N. Salankar and S. M. Qaisar, "EEG based stress classification by using difference plots of variational modes and machine learning," *Journal of Ambient Intelligence and Humanized Computing*, vol. 14, no. 12, pp. 16347-16360, 2023.
- [12] M. Soufneyestani, D. Dowling, and A. Khan, "Electroencephalography (EEG) technology applications and available devices," *Applied Sciences*, vol. 10, no. 21, p. 7453, 2020.

- [13] M.-S. Song, S.-G. Kang, K.-T. Lee, and J. Kim, "Wireless, skin-mountable EMG sensor for human-machine interface application," *Micromachines*, vol. 10, no. 12, p. 879, 2019.
- [14] G. Lu, F. Yang, J. A. Taylor, and J. F. Stein, "A comparison of photoplethysmography and ECG recording to analyse heart rate variability in healthy subjects," *Journal of medical engineering & technology*, vol. 33, no. 8, pp. 634-641, 2009.
- [15] M. A. Serhani, H. T. El Kassabi, H. Ismail, and A. Nujum Navaz, "ECG monitoring systems: Review, architecture, processes, and key challenges," *Sensors*, vol. 20, no. 6, p. 1796, 2020.
- [16] S. S. Bipro, S. Kabir, and M. A. Motin, "Monitoring Stress Using Electrocardiogram Signal," in *2023 Computing in Cardiology (CinC)*, 2023, vol. 50: IEEE, pp. 1-4.
- [17] M. Masoumian Hosseini, S. T. Masoumian Hosseini, K. Qayumi, S. Hosseinzadeh, and S. S. Sajadi Tabar, "Smartwatches in healthcare medicine: assistance and monitoring; a scoping review," *BMC Medical Informatics and Decision Making*, vol. 23, no. 1, p. 248, 2023.
- [18] M. A. Motin, C. Karmakar, M. Palaniswami, and T. Penzel, "Photoplethysmographic-based automated sleep-wake classification using a support vector machine," *Physiological Measurement*, vol. 41, no. 7, p. 075013, 2020.
- [19] M. A. Motin, C. K. Karmakar, and M. Palaniswami, "Ensemble empirical mode decomposition with principal component analysis: A novel approach for extracting respiratory rate and heart rate from photoplethysmographic signal," *IEEE journal of biomedical and health informatics*, vol. 22, no. 3, pp. 766-774, 2017.
- [20] M. A. Motin, C. K. Karmakar, and M. Palaniswami, "Selection of empirical mode decomposition techniques for extracting breathing rate from PPG," *IEEE Signal Processing Letters*, vol. 26, no. 4, pp. 592-596, 2019.
- [21] M. A. Motin, C. K. Karmakar, T. Penzel, and M. Palaniswami, "Sleep-Wake Classification using Statistical Features Extracted from Photoplethysmographic Signals," in *2019 41st Annual International Conference of the IEEE Engineering in Medicine and Biology Society (EMBC)*, 2019: IEEE, pp. 5564-5567.
- [22] K. B. Kim and H. J. Baek, "Photoplethysmography in wearable devices: a comprehensive review of technological advances, current challenges, and future directions," *Electronics*, vol. 12, no. 13, p. 2923, 2023.
- [23] A. Alqaraawi, A. Alwosheel, and A. Alasaad, "Heart rate variability estimation in photoplethysmography signals using Bayesian learning approach," *Healthcare technology letters*, vol. 3, no. 2, pp. 136-142, 2016.
- [24] M. Benchekroun *et al.*, "Comparison of Stress Detection through ECG and PPG signals using a Random Forest-based Algorithm," in *2022 44th Annual International Conference of the IEEE Engineering in Medicine & Biology Society (EMBC)*, 2022: IEEE, pp. 3150-3153.
- [25] H. Kim *et al.*, "Machine learning-based classification analysis of knowledge worker mental stress," *Frontiers in Public Health*, vol. 11, p. 1302794, 2023.
- [26] S. Heo, S. Kwon, and J. Lee, "Stress detection with single PPG sensor by orchestrating multiple denoising and peak-detecting methods," *IEEE Access*, vol. 9, pp. 47777-47785, 2021.
- [27] Y. S. Can, N. Chalabianloo, D. Ekiz, and C. Ersoy, "Continuous Stress Detection Using Wearable Sensors in Real Life: Algorithmic Programming Contest Case Study," *Sensors*, vol. 19, no. 8, p. 1849, 2019. [Online]. Available: <https://www.mdpi.com/1424-8220/19/8/1849>.
- [28] A. Bellante *et al.*, "Emocyc: Towards physiological signals-based stress detection," in *2021 IEEE EMBS International Conference on Biomedical and Health Informatics (BHI)*, 2021: IEEE, pp. 1-4.
- [29] L. Zhu, P. Spachos, and S. Gregori, "Multimodal physiological signals and machine learning for stress detection by wearable devices," in *2022 IEEE International Symposium on Medical Measurements and Applications (MeMeA)*, 2022: IEEE, pp. 1-6.
- [30] W.-K. Beh, Y.-H. Wu, and A.-Y. Wu, "Robust PPG-based mental workload assessment system using wearable devices," *IEEE Journal of Biomedical and Health Informatics*, vol. 27, no. 5, pp. 2323-2333, 2021.
- [31] R. Li and Z. Liu, "Stress detection using deep neural networks," *BMC Medical Informatics and Decision Making*, vol. 20, pp. 1-10, 2020.
- [32] S. Elzeiny and M. Qaraqe, "Stress classification using photoplethysmogram-based spatial and frequency domain images," *Sensors*, vol. 20, no. 18, p. 5312, 2020.
- [33] Y. Hasanpoor, K. Motaman, B. Tarvirdizadeh, K. Alipour, and M. Ghamari, "Stress detection using ppg signal and combined deep cnn-mlp network," in *2022 29th National and 7th International Iranian Conference on Biomedical Engineering (ICBME)*, 2022: IEEE, pp. 223-228.
- [34] F. Gasparini, A. Grossi, and S. Bandini, "A deep learning approach to recognize cognitive load using ppg signals," in *Proceedings of the 14th Pervasive Technologies Related to Assistive Environments Conference*, 2021, pp. 489-495.
- [35] P. Kalra and V. Sharma, "Mental stress assessment using PPG signal a deep neural network approach," *IETE Journal of Research*, vol. 69, no. 2, pp. 879-885, 2023.
- [36] N. Rashid, L. Chen, M. Dautta, A. Jimenez, P. Tseng, and M. A. Al Faruque, "Feature augmented hybrid cnn for stress recognition using wrist-based photoplethysmography sensor," in *2021 43rd Annual International Conference of the IEEE Engineering in Medicine & Biology Society (EMBC)*, 2021: IEEE, pp. 2374-2377.
- [37] Q. Chen and B. G. Lee, "Deep learning models for stress analysis in university students: a sudoku-based study," *Sensors*, vol. 23, no. 13, p. 6099, 2023.
- [38] M. Alshamrani, "An Advanced Stress Detection Approach based on Processing Data from Wearable Wrist Devices," *International Journal of Advanced Computer Science and Applications(IJACSA)*, vol. 12(7), 2021, doi: <https://dx.doi.org/10.14569/IJACSA.2021.0120745>.
- [39] Y. LeCun, Y. Bengio, and G. Hinton, "Deep learning," *Nature*, vol. 521, no. 7553, pp. 436-444, 2015/05/01 2015, doi: 10.1038/nature14539.
- [40] A. Habib, M. A. Motin, T. Penzel, M. Palaniswami, J. Yearwood, and C. Karmakar, "Performance of a convolutional neural network derived from PPG signal in classifying sleep stages," *IEEE Transactions on Biomedical Engineering*, vol. 70, no. 6, pp. 1717-1728, 2022.
- [41] P. Schmidt, V. Marber, R. Duerichen, C. Marberger, and K. Van Laerhoven, "Introducing wesad, a multimodal dataset for wearable stress and affect detection," in *Proceedings of the 20th ACM international conference on multimodal interaction*, 2018, pp. 400-408.
- [42] I. Albuquerque *et al.*, "Wauc: a multi-modal database for mental workload assessment under physical activity," *Frontiers in Neuroscience*, vol. 14, p. 549524, 2020.
- [43] V. Markova, T. Ganchev, and K. Kalinkov, "Clas: A database for cognitive load, affect and stress recognition," in *2019 International Conference on Biomedical Innovations and Applications (BIA)*, 2019: IEEE, pp. 1-4.
- [44] W.-K. Beh and Y.-H. Wu, "MAUS: A dataset for mental workload assessment N-back task using wearable sensor," *arXiv preprint arXiv:2111.02561*, 2021.
- [45] J. R. Stroop, "Studies of interference in serial verbal reactions," *Journal of experimental psychology*, vol. 18, no. 6, p. 643, 1935.
- [46] W. Rauch and K. Schmitt, "Fatigue of cognitive control in the stroop-task," in *Proceedings of the annual meeting of the cognitive science society*, 2009, vol. 31, no. 31.
- [47] M. Gergelyfi, B. Jacob, E. Olivier, and A. Zénon, "Dissociation between mental fatigue and motivational state during prolonged mental activity," *Frontiers in behavioral neuroscience*, vol. 9, p. 176, 2015.
- [48] H. Weiqi, F. Y. Kai, C. Zhi-En, A. A. P. Wai, and C. Sher-Yi, "Multimodal Sensory Headband for Personalized Relaxation Management," in *i-CREATE 2015 Proceedings of the international Convention on Rehabilitation Engineering Assistive Technology. Singapore Therapeutic, Assistive Rehabilitative Technologies (START) Centre, Kaki Bukit TechPark II, Singapore, Article*, 2015, vol. 9.
- [49] J. M. Johnson and T. M. Khoshgoftaar, "Survey on deep learning with class imbalance," *Journal of big data*, vol. 6, no. 1, pp. 1-54, 2019.
- [50] G. Hinton, N. Srivastava, and K. Swersky, "Neural networks for machine learning lecture 6a overview of mini-batch gradient descent," *Cited on*, vol. 14, no. 8, p. 2, 2012.
- [51] S.-A. Rebuffi, S. Gowal, D. A. Calian, F. Stimberg, O. Wiles, and T. A. Mann, "Data augmentation can improve robustness," *Advances in Neural Information Processing Systems*, vol. 34, pp. 29935-29948, 2021.
- [52] S. Hu, W. Cai, T. Gao, and M. Wang, "A hybrid transformer model for obstructive sleep apnea detection based on self-attention mechanism using single-lead ECG," *IEEE Transactions on Instrumentation and Measurement*, vol. 71, pp. 1-11, 2022.
- [53] A. Jahanjoo, N. TaheriNejad, and A. Aminifar, "High-Accuracy Stress Detection Using Wrist-Worn PPG Sensors," in *2024 IEEE International Symposium on Circuits and Systems (ISCAS)*, 19-22 May 2024 2024, pp. 1-5, doi: 10.1109/ISCAS58744.2024.10558012.
- [54] L. McInnes, J. Healy, and J. Melville, "Umap: Uniform manifold approximation and projection for dimension reduction," *arXiv preprint arXiv:1802.03426*, 2018.
- [55] H. Meng, C. Wagner, and I. Triguero, "Explaining time series classifiers through meaningful perturbation and optimisation," *Information Sciences*, vol. 645, p. 119334, 2023.

## Pre-print

- [56] J. Ahn, H.-K. Ra, H. J. Yoon, S. H. Son, and J. Ko, "On-device filter design for self-identifying inaccurate heart rate readings on wrist-worn ppg sensors," *IEEE Access*, vol. 8, pp. 184774-184784, 2020.
- [57] T. F. Beutel, R. Zwerenz, and M. Michal, "Psychosocial stress impairs health behavior in patients with mental disorders," *BMC psychiatry*, vol. 18, pp. 1-13, 2018.